sample 2.1 W/cm^2 of unpolarized collimated light having a typical Hg arc lamp spectrum. See *Oriel Catalogue* (Oriel, Stratford, CT, 1994), vol. 2, pp. 1–41.

22. P. G. deGennes, J. Prost, *The Physics of Liquid Crystals* (Oxford, London, 1993).
23. E31 is a mixture of cyanobiphenyl homologs, primarily 5-8CB, for which K_B, K_S, and K_T are, respectively, ≈ 25, 17.5, and 8.5 pN (*22*).
24. R. Stannarius, in *Handbook of Liquid Crystals*, D. Demaus *et al.*, Eds. (Wiley-VCH Weinheim, Berlin, 1998), chap. 2.1.
25. B. W. Lee, thesis, University of Colorado, 1998 (Dissertation Abstracts no. 9838378).
26. Addition to the free energy of saddle-splay elasticity, the tendency for opposite sign of splay in orthogonal planes parallel to **n** (*24, 25*), will cause a rotation of **n** away from the boundary line, the tip of **n** furthest from the surface rotating toward the GLASS region (Fig. 2).
27. We are now in a position to compare this boundary-alignment energy with that arising from the $\delta h \sim 1$ nm surface relief at the SAM-GLASS boundaries. The latter can be obtained from the Berreman formula $\gamma_{\text{relief}} \sim 2\pi^3 K(\delta h/w)^2$ (*7*), where $w \sim 100$ nm is the width of the SAM-GLASS boundary region, determined by the wavelength of the UV writing light and measured by AFM in figure 6 of (*17*). $\gamma_{\text{relief}} \sim 10^{-3}\gamma_{\text{BI}}$ and is thus negligible.
28. The HO-RP boundary positions match the mask boundary positions to within 0.1 μm, as verified by AFM. See (*17*).
29. M. Schadt, W. Helfrich, *Appl. Phys. Lett.* **18**, 127 (1971).
30. CB15 is the British Drug House designation for chiral 4-cyano-4′-(2-methyl)butyl-biphenyl.
31. A. Kumar, N. L. Abbot, H. A. Biebucyk, G. M. Whitesides, *Acc. Chem. Res.* **28**, 219 (1995).
32. K. Ichimura, *Supramol. Sci.* **3**, 67 (1996).

33. Supported by NSF Materials Research Science and Engineering Centers (grant DMR 98-09555) and Army Research Office (grant DAAG55-98-1-0046).

30 November 2000; accepted 27 February 2001

Quantitative Measurement of Short-Range Chemical Bonding Forces

M. A. Lantz,* H. J. Hug, R. Hoffmann, P. J. A. van Schendel, P. Kappenberger, S. Martin, A. Baratoff, H.-J. Güntherodt

We report direct force measurements of the formation of a chemical bond. The experiments were performed using a low-temperature atomic force microscope, a silicon tip, and a silicon (111) 7×7 surface. The measured site-dependent attractive short-range force, which attains a maximum value of 2.1 nanonewtons, is in good agreement with first-principles calculations of an incipient covalent bond in an analogous model system. The resolution was sufficient to distinguish differences in the interaction potential between inequivalent adatoms, demonstrating the ability of atomic force microscopy to provide quantitative, atomic-scale information on surface chemical reactivity.

The atomic force microscope (AFM) was originally intended to be a tool capable of measuring the forces acting between a single pair of atoms (*1*) but has only recently evolved into an instrument capable of producing atomically resolved images of surfaces with characteristic features and defects (*2–4*). This true atomic-scale contrast is generally interpreted as resulting from the short-range chemical interaction between an atomically sharp AFM tip and the nearest atoms on the surface of the sample. In principle, it should therefore be possible to map the chemical bonding potential between the foremost atom on an AFM tip and a specific atom on the sample.

The measurement of short-range bonding forces with the AFM has been difficult to achieve for several reasons. First, at room temperature, thermal drift and piezoelectric scanner creep make it difficult to reliably position the tip above a specific lattice position. Second, most atomic-resolution AFM images have been obtained using a dynamic technique in which the tip-bearing cantilever is driven on its fundamental resonant frequency with a typical amplitude of several nanometers. When the cantilever tip comes close to the sample surface, the force acting on the tip weakly perturbs the cantilever oscillation, giving rise to a small shift Δf in the resonance frequency. The frequency shift is used as a feedback parameter to control the tip-sample spacing, and images therefore correspond to contours of constant frequency shift. Because of the large tip excursion, the relation between the measured frequency shift and the force acting on the tip is not straightforward. Recently, however, progress has been made in quantitatively understanding and inverting this relation (*5–9*). A third difficulty arises because, in general, both short-range forces (such as covalent bonding forces) and long-range forces [such as van der Waals (vdW) and electrostatic forces] act on the tip. Separating these contributions in order to isolate the short-range chemical bonding force is a nontrivial problem. Finally, it is difficult to determine whether the measured chemical force involves more than just a single pair of atoms.

Previously, we demonstrated that the problems of drift and creep can be overcome by working at low temperatures (*10*). In that preliminary work, we acquired constant-height images of the Si(111) 7×7 surface at five tip-sample distances and used the data to construct approximate frequency-versus-distance curves above specific lattice positions. The five data points measured above an adatom site were compared with a frequency shift curve calculated using a first-principles simulation of the short-range force and a simple model for the long-range force. The data were found to be in reasonable agreement with the model, allowing estimation of the maximum attractive force acting on the tip.

Here, we describe quantitative measurements of the short-range chemical bonding force acting between the apex of a silicon AFM tip and specific atomic sites on a Si(111) 7×7 sample. The force is measured over a large range of tip-sample distances using site-specific frequency-distance measurements, which we convert to force-distance data with the use of a recently developed inversion procedure (*7*). The short- and long-range forces are accurately separated by compensating the electrostatic force and measuring the vdW force above nonreactive sites. The magnitude and range of the measured short-range force are found to be in good agreement with first-principles calculations designed to model the same situation (*11*). In addition, we demonstrate that the measured short-range force results from the formation of a single bond. These measurements provide insight into covalent bond formation at surfaces and have implications for understanding the mechanisms responsible for contrast formation in true atomic-resolution AFM.

The experiments were performed using a commercial silicon cantilever, a p-type silicon sample prepared in situ by direct-current heating, and a home-built low-temperature AFM operating in an ultrahigh vacuum (UHV) environment (*10, 12*). After transfer into the UHV system, the cantilever (*13*) was heated to 150°C for 2 hours to remove absorbed contaminants. To preserve the sharpness of the tip, we applied no additional cleaning procedures; thus, we assume that the tip was initially covered with a native oxide layer. After the microscope was cooled to 7.2 K, imaging was performed in the constant Δf dynamic mode using a constant cantilever oscillation am-

---

Institute of Physics, University of Basel, Klingelbergstrasse 82, CH-4056 Basel, Switzerland.

*To whom correspondence should be addressed. E-mail: mark.lantz@unibas.ch

plitude of 6.1 nm. Upon first imaging the sample, we observed weak contrast reflecting the unit cell periodicity. We have found this weak contrast to be typical when imaging the Si(111) 7×7 surface with an untreated tip. With continued scanning, an abrupt improvement in contrast occurred, after which the individual adatoms were clearly resolved. We have previously observed similar abrupt changes in contrast and attributed them to the transfer of one or more silicon atoms from the sample onto an oxide-terminated tip (*10, 14*).

In our experimental procedure for measuring the tip-sample interaction, we begin by obtaining an atomically resolved image of the surface near the center of a terrace. After image acquisition, the displacement feedback is turned off, and the sample is retracted by a preset distance and positioned above a specific lattice position determined from the atomically resolved image. The shift in resonance frequency is then recorded while the sample is ramped toward the tip by a fixed distance. While positioning the tip above different sites, the average plane of the sample surface (determined during the initial imaging procedure) is taken into account to ensure the same relative starting position for each measurement. After a series of measurements, the tip is returned to its original position, the sample displacement feedback is reactivated, and the surface is imaged to determine whether the tip or sample has been modified and to ensure that no detectable drift occurred.

The force acting on the tip at the distance of closest approach to the sample during an oscillation cycle was calculated from the Δf-versus-distance data using the procedure described by Dürig (*7*). The force calculated in this way is a well-defined function of the sample displacement. In the distance regime where atomic-resolution images are obtained, there are potentially three distinct forces acting on the tip: a strongly site-dependent short-range force as well as long-range electrostatic and vdW forces. The latter are considered site independent, because they are dominated by contributions from many atoms, and hence can be computed to a good approximation by integrating over the volumes of the sample and the tip (*15*). The long-range electrostatic force arises predominantly from the contact potential difference between the tip and sample, which can be minimized by applying a compensating voltage (*8*). For the experiments described here, this was achieved by applying +1.16 V to the sample, and we therefore expect that only the vdW contribution remains. To separate the short-range interaction, we took advantage of the special features of the Si(111) 7×7 surface (*16*). Above the corner hole site, the tip apex stays relatively far from any of the dangling bonds on the surface (>6.65 Å from the surrounding adatoms at the distance of closest approach), and we therefore assume that the measured frequency shift results only from the site-independent vdW interaction (see Fig. 1A). Above the adatoms, the frequency shift results from both long- and short-range forces. Assuming that the forces are additive, we isolate the force due to the short-range interaction by subtracting the long-range force calculated from the data measured above the corner hole from the total force measured above an adatom site.

An image of the surface acquired at a preset frequency shift of –38 Hz is shown in Fig. 1B. After acquisition, frequency-distance measurements were performed above the center of the corner hole site labeled 1, and above the two inequivalent adatom sites labeled 2 and 3. At a given site, the sample was retracted by 63.07 Å and ramped forward a distance of 64.33 Å at a rate of 6 Å/s in order to characterize the long-range force regime. Then, to investigate the short-range force regime with a higher density of data points, we retracted the sample 15.77 Å and then ramped it forward 17.03 Å at a rate of 1.7 Å/s (the minimum tip-sample distance is therefore less than the initial distance by 1.26 Å). During each approach, 512 data points were acquired. An example of data acquired above the three sites is shown in Fig. 2A. We have plotted the data in terms of both Δf and the normalized frequency shift $\gamma = \Delta f k A_0^{3/2}/f_0$, where k is the spring constant of the cantilever, A_0 is the amplitude of oscillation, and f_0 is the resonance frequency (*5*). The choice of the zero position on the horizontal axis is somewhat arbitrary (see below). At distances greater than ~12 Å, the Δf data measured above the three sites are virtually identical, as expected for the long-range component of the force. At small tip-sample distances, Δf measured above the adatom sites drops much faster than above the corner hole, which is consistent with a strong, site-dependent short-range force. Furthermore, the magnitude and range of γ due to short-range forces (i.e., the difference between γ measured above the adatom and above the corner hole site) are consistent with our previous data extracted from constant-height scans, measured using a cantilever with a smaller spring constant (*10, 17*). Roughly similar rapid changes in Δf have been reported in room-temperature experiments on Si(111) 7×7 samples, typically at poorly defined sites (*18, 19*) and recently above adatoms (*20*), but no attempts were made to extract quantitative site-dependent forces from the data.

The tip-sample interaction force calculated from the data measured above the corner hole is shown in Fig. 2B (*21*). To test the validity of our assumption that only vdW forces are acting above the corner hole, we compare the measured force with a Hamaker-like analytic model. In our previous work (*10*), a reliable comparison was not possible because of the limited distance range over which the long-range force was measured and because the electrostatic forces were not compensated (*22*). For a sphere-plane geometry, the vdW force, to a good approximation, is given by F_{vdW} =

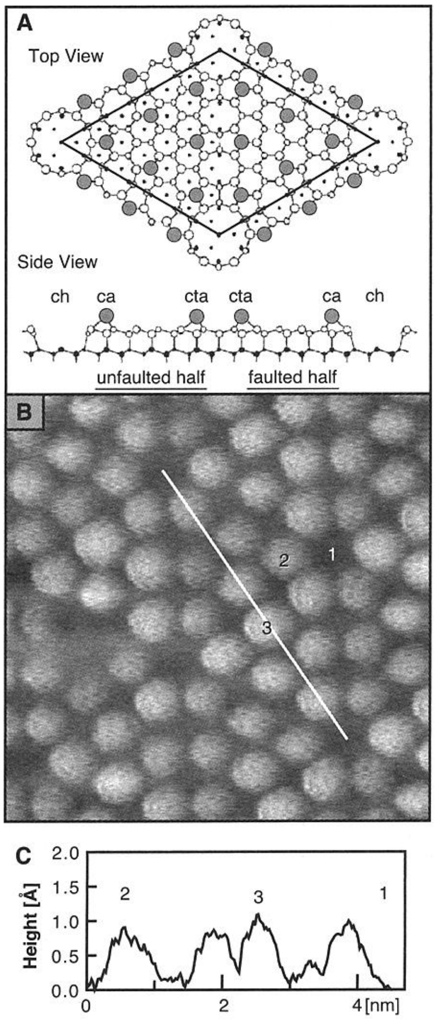

Fig. 1. (**A**) Dimer adatom stacking-fault model of the Si(111) 7×7 surface (*16*). The unit cell is outlined by a black diamond. The adatoms are shown as gray circles; the side view shows the positions of the corner holes (ch), corner adatoms (ca), and center adatoms (cta). (**B**) Constant frequency shift image (Δf = –38 Hz, root mean square error 1.15 Hz, scan speed 2 nm/s, image size 6 nm by 6 nm). The labels 1, 2, and 3 indicate the position of frequency distance measurements (see text). The white line indicates the position of the line section shown in (**C**). The corner hole position labeled 1 and the corner adatom labeled 2 in the line section are equivalent by trigonal symmetry to sites 1 and 2 in (A).

$-A_H R/6(z + z_0)^2$, for $z + z_0 < R$ (*23*), where A_H is the Hamaker constant, R is the mesoscopic tip radius, z is the sample displacement, and z_0 is a constant that accounts for the height of the absorbed atom or cluster on the tip apex. In addition, z_0 accounts for the uncertainty in the absolute distance between the tip and sample and the density of atoms in the top layer being lower than in the bulk. We have taken $A_H R$ and z_0 as fitting parameters, and we find an excellent fit to the data using $A_H R = 9.1 \times 10^{-28}$ J·m and $z_0 = 1.0$ Å (see Fig. 2B) (*24*). The quality of the fit confirms our assumption that vdW forces dominate the tip-sample interaction above the corner hole.

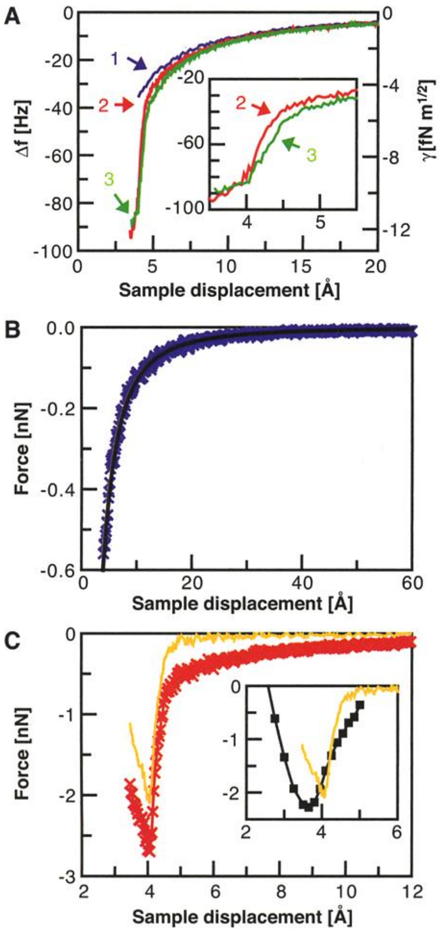

Fig. 2. (**A**) Frequency shift Δf and normalized frequency shift γ versus distance, as measured above the positions labeled 1, 2, and 3 in Fig. 1B. The inset adjusts the scales for Δf and distance to give a better picture of the data acquired above the two inequivalent adatoms. (**B**) Force-distance relation determined above the corner hole (blue symbols) and a fit to the data using a sphere-plane model for the vdW force (black line). (**C**) Total force (red line with symbols) and short-range force (yellow line) determined above the adatom site labeled 2 in Fig. 1. In the inset, the measured short-range force is compared with a first-principles calculation (black line with symbols) (*11*).

Inverting the Δf data measured above adatom site 2 yields the force shown in Fig. 2C, which includes both long- and short-range components. The short-range force due to the chemical interaction was determined by subtracting the long-range force measured above the corner hole. To avoid increasing the noise in the data, we have subtracted the fit shown in Fig. 2B rather than the raw data. In the inset of Fig. 2C, we compare the measured short-range force with the force reported by Perez *et al.* (*11*), who calculated the bonding interaction between a model Si nanotip composed of 10 atoms and terminated by a single atom with one dangling bond directed toward an adatom on the Si(111) 5×5 surface. They found that the predominantly covalent bond formation between these atoms results in relaxation of the positions of the foremost atoms in the tip and sample at small separations. These relaxation effects are important because we measure the sample displacement and not the actual distance between the apex atom and the adatom, which exhibits a nonlinear deviation from the sample displacement as a consequence of relaxation. In plotting our experimental data, we have chosen the zero point on the sample displacement axis for consistency with the data of Perez *et al.*, plotted in a similar fashion (i.e., curve FAd in their figure 3). Comparing the two curves in the region where the attractive force increases with decreasing distance, we notice that the slope of the measured force is steeper than that of their calculated force, indicating that the relaxation effects in our experiment are larger than those calculated by Perez *et al.* As noted previously (*10*), this difference is not surprising because the actual tip and sample are much more extended, and hence subject to larger overall deformations, than the slab and cluster used in their density functional theory calculations. In the range beyond the maximum attractive force, the slope of the measured force appears less steep than the slope of the calculated force; this is also consistent with additional relaxation. The uncertainty in the magnitude of the measured force arises mainly from the uncertainties in the oscillation amplitude and in the spring constant of the cantilever. Considering the resulting uncertainty in the measured force (about ±30%), the measured maximum attractive force (–2.1 nN) is in remarkably good agreement with the calculated force (–2.25 nN). The reproducibility of the measurements was excellent; that is, measurements above the same sites were indistinguishable to within the noise level of the measurement. This indicates that the tip and sample were not modified in the course of the experiments (*25*).

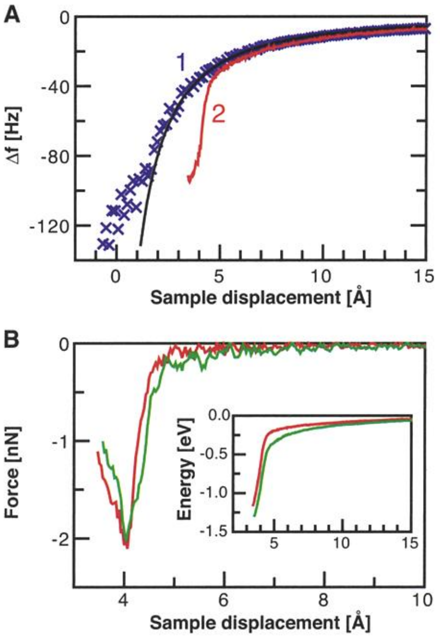

Fig. 3. (**A**) Frequency shift measured above the corner hole (symbols) and extrapolated from the model fit to the data of Fig. 2B (blue line). For comparison, the data acquired above adatom site 2 from Fig. 2A are also plotted (red line). (**B**) Short-range force and interaction energy (inset) measured above the sites labeled 2 and 3 in Fig. 1.

The short decay length of the measured short-range force and the good agreement between the magnitudes of the calculated and measured short-range force indicate that the measurement indeed corresponds to the formation of a single covalent bond. We can also experimentally test whether other reactive sites on the tip contribute to the measured force by performing additional measurements above the corner hole, probing several angstroms below the point of maximum attractive force measured above the adatoms. The result of such an experiment is shown in Fig. 3A. To determine the displacement range over which purely vdW forces are acting, we have calculated the frequency shift over the measured range using the vdW model fit to the data of Fig. 2B, and plotted the corresponding curve in Fig. 3A (for comparison, we have also plotted the data measured above adatom site 2). The fit and the data measured above the corner hole are in excellent agreement down to a sample displacement of ~2 Å, which is ~1.5 Å below the point of closest approach above the adatom. If there were additional dangling bonds close enough to the end of the tip to interact with the sample, Δf should decrease more rapidly than predicted by the vdW model. However, for sample displacements below ~2 Å, Δf decreases much less rapidly than predicted by the vdW model, indicating the onset of a strong short-range repulsive force that probably results from the proximity of the mesoscopic oxide tip to the adatoms surrounding the corner hole. The good agreement between the vdW model and the data, down to the onset of these repulsive forces, indicates that no other dangling bonds on the tip contribute to the short-range force measured above the adatoms. We conclude that the short-range force data in Fig. 2C arise from a single incipient covalent bond forming between the tip apex atom and the nearest adatom on the surface.

In the image and line section shown in Fig. 1, height differences are clearly observed between the inequivalent adatom sites. This contrast is qualitatively consistent with our previous work (*10*), and as before, we find that these relative height differences, as well as the overall corrugation, are dependent on the frequency shift set point used for imaging. First-principles calculations predict tiny height differences between the inequivalent adatom positions [less than 0.1 Å, the corner adatoms in the faulted half of the unit cell (see Fig. 1A) being the highest] (*26*). These differ from the larger height differences observed in Fig. 1C and in previous AFM studies (*19, 27–29*). Clearly, the observed differences cannot be due to purely geometric effects, but rather reflect differences in the interaction potential above inequivalent sites. We have performed frequency-versus-distance measurements above the two sites (2 and 3) that exhibit the largest height differences in the line section shown in Fig. 1C (see Fig. 2A). Note that site 2 in Fig. 1B is equivalent by trigonal symmetry to the adatom labeled 2 in Fig. 1C. The short-range force calculated from the frequency data is shown in Fig. 3B. The two force curves appear similar except for subtle differences near the onset of the short-range attractive force. Nevertheless, these differences are important because the image shown in Fig. 1B was acquired in the weak interaction regime (i.e., at $\Delta f \approx -38$ Hz), which corresponds to a short-range force of about -0.24 nN above site 2 and -0.17 nN above site 3. These differences in the interaction potential above inequivalent adatom sites were consistently observed in repeated measurements. They are manifested more clearly in the raw Δf data or if we calculate the short-range interaction energy by integrating the unsmoothed force data with respect to the sample displacement (Fig. 3B, inset). Note that because of relaxation effects, the dependence plotted in Fig. 3B is not the binding energy versus interatomic distance.

The observed differences in the interaction energy are most likely due to variations in the charge distribution among inequivalent adatom sites. According to first-principles calculations (*26, 30*), such variations are already present on the free Si(111) 7×7 surface. Our observed height differences between inequivalent adatoms show trends similar to the calculated distribution of electronic charge. The differences in the interaction force and energy measured above inequivalent adatom sites can also be thought of as variations in the reactivity of these sites. Such differences have been predicted using first-principles calculations, but experimentally they have only been observed indirectly (*31*). It is also interesting that at larger tip-sample separations, the measured short-range force and energy decay much more slowly than expected for a purely covalent interaction. The tails in question are likely due to electrostatic interactions, which remain even if the average contact potential between the tip and sample is compensated. Because of the different local environments of adatoms and of the apex atom of the tip, the bond formed contains a small ionic component. A test charge above the sample would sense an exponentially decaying potential with the longest decay length given by $\sqrt{3}a/4\pi = 3.71$ Å, where $a = 26.9$ Å is the lattice constant of the 7×7 reconstruction.

The measurements presented here demonstrate the possibility of directly measuring and quantifying local surface reactivity with the AFM. The range of systems that can be studied by such measurements could be extended by depositing different materials or even single atoms on the tip. The resolution of our measurements was sufficient to reveal differences in the interaction potential between inequivalent Si adatoms; hence, it may eventually be possible to use similar methods to distinguish between different atomic species, as proposed previously (*32, 33*), or to measure exchange forces.

References and Notes

1. G. Binnig, C. F. Quate, C. Gerber, *Phys. Rev. Lett.* **56**, 930 (1986).
2. F. Ohnesorge, G. Binnig, *Science* **260**, 1451 (1993).
3. F. J. Giessibl, *Science* **267**, 68 (1995).
4. S. Kitamura, M. Iwatsuki, *Jpn. J. Appl. Phys.* **34**, 145 (1995).
5. F. J. Giessibl, *Phys. Rev. B* **56**, 16010 (1997).
6. B. Gotsmann, B. Anczykowski, C. Seidel, H. Fuchs, *Appl. Surf. Sci.* **140**, 314 (1999).
7. U. Dürig, *Appl. Phys. Lett.* **76**, 1203 (2000).
8. M. Guggisberg *et al.*, *Phys. Rev. B* **61**, 11151 (2000).
9. F. J. Giessibl, *Appl. Phys. Lett.* **78**, 123 (2001).
10. M. A. Lantz *et al.*, *Phys. Rev. Lett.* **84**, 2642 (2000).
11. R. Perez, I. Stich, M. C. Payne, K. Terakura, *Phys. Rev. B* **58**, 10835 (1998).
12. H. J. Hug *et al.*, *Rev. Sci. Instrum.* **70**, 3625 (1999).
13. The fundamental resonance frequency f_0 and Q-factor (which describes the width of the resonance peak) of the cantilever, measured at 7.2 K, were 172,509.55 Hz and 522,800, respectively. The spring constant, as specified by the manufacturer (Nanosensors), was $k = 48$ N/m.
14. A. Abdurixit *et al.*, in preparation.
15. J. Israelachvili, *Intermolecular and Surface Forces* (Academic Press, London, ed. 2, 1992).
16. K. Takayanagi, Y. Tanishiro, M. Takahashi, S. Takahashi, *J. Vac. Sci. Technol. A* **3**, 1502 (1985).
17. Note that the sample displacement scales in (*10*) must be multiplied by a factor of 1.48 because of a piezoelectric scanner calibration error.
18. R. Lüthi *et al.*, *Surf. Rev. Lett.* **4**, 1025 (1997).
19. T. Uchihashi *et al.*, *Phys. Rev. B* **56**, 9834 (1997).
20. S. Morita, Y. Sugawara, K. Yokoyama, T. Uchihashi, *Nanotechnology* **11**, 1 (2000).
21. The procedure used for calculating the force (*7*) involves taking the numerical derivative of the frequency shift data, which increases the noise in the calculated force. To reduce this effect, we have smoothed the force data using a running average of five data points. All of the force data presented here were calculated using three iterations, which was sufficient to obtain convergence to >95% accuracy (i.e., better than the noise level of the measurements).
22. In (*10*), we assumed a purely conical tip shape to model the long-range forces acting on the tip. However, we note that for the small tip-sample displacements (~1 Å) over which the long-range force was measured, equally good agreement could be obtained using either a conical or a spherical tip model. In the present work, good agreement could only be obtained using a spherical tip model.
23. C. Argento, R. H. French, *J. Appl. Phys.* **80**, 6081 (1996).
24. Taking the fitted value of $A_H R$, we can estimate the radius of the tip using reported values of A_H. For an SiO_2 tip, we estimate A_H for the tip-sample system as the geometric mean of A_H for Si and SiO_2 (*15*). Taking $A_{H\text{-}Si} = 0.1865$ aJ (*34*) and $A_{H\text{-}SiO_2} = 0.065$ aJ (*15*) yields $R = 8.3$ nm, which is consistent with the manufacturer's specification of $R \leq 10$ nm. For a Si tip (i.e., taking $A_H = 0.1865$ aJ), we find $R = 4.9$ nm. Because the native oxide covering the tip is probably only a few nanometers thick, the actual radius probably lies between these values. In any case, we conclude that the mesoscopic tip is extremely sharp.
25. At small tip-sample distances, we observed that the excitation signal required to keep the tip oscillation amplitude constant above an adatom site increased, indicating an onset of dissipation induced by the short-range interaction (i.e., a breakdown of adiabaticity). This observation, together with the abrupt change in slope of the short-range attractive force, may indicate an instability, most likely in the position of the foremost atom on the tip. However, the increase in energy dissipated per oscillation cycle is still small compared to the total Si-Si covalent bond energy. Thus, even if such an instability occurs, we do not expect it to have a large effect on the measured interaction force.
26. K. D. Brommer, M. Needels, B. E. Larson, J. D. Joannopoulos, *Phys. Rev. Lett.* **68**, 1355 (1992).
27. R. Erlandsson, L. Olsson, P. Martensson, *Phys. Rev. B* **54**, R8309 (1996).
28. N. Nakagiri, M. Suzuki, K. Okiguchi, H. Sugimura, *Surf. Sci.* **373**, L329 (1997).
29. F. J. Giessibl, S. Hembacher, H. Bielefeldt, J. Mannhart, *Science* **289**, 422 (2000).
30. I. Stich, M. C. Payne, R. D. King-Smith, J.-S. Lin, *Phys. Rev. Lett.* **68**, 1351 (1992).
31. K. D. Brommer, M. Galvan, J. A. Dal Pino, J. D. Joannopoulos, *Surf. Sci.* **314**, 57 (1994).
32. S. P. Jarvis *et al.*, *Nature* **384**, 247 (1996).
33. K. Yokoyama, T. Ochi, Y. Sugawara, S. Morita, *Phys. Rev. Lett.* **83**, 5023 (1999).
34. T. J. Senden, C. J. Drummond, *Colloids Surf.* **A94**, 29 (1995).
35. We thank U. Dürig and A. Abdurixit for helpful discussions, and C. Loppacher and M. Guggisberg for assistance with the data acquisition software. Supported in part by the Swiss National Research Program NFP 36.

28 November 2000; accepted 13 February 2001